

Singlet Oxygen in Microporous Silica Xerogel: Quantum Yield and Oxidation at the Gas–Solid Interface

Christophe Cantau,^[a] Thierry Pigot,^[a] Narayanapillai Manoj,^[b] Esther Oliveros,^[b] and Sylvie Lacombe^{*[a]}

The quantum yields of singlet oxygen ($^1\text{O}_2$) production (Φ_{Δ}) and $^1\text{O}_2$ lifetimes (τ_{Δ}) at the gas–solid interface in silica gel material are determined. Different photosensitizers (PS) are encapsulated in parallelepipedic xerogel monoliths (PS-SG). PS were chosen according to their known photooxidation properties: 9,10-dicyanoanthracene (DCA), 9,10-anthraquinone (ANT), and a benzophenone derivative, 4-benzoyl benzoic acid (4BB). These experiments are mainly based on time-resolved $^1\text{O}_2$ phosphorescence detection, and the obtained Φ_{Δ} and τ_{Δ} values are compared with those of a reference sensitizer for $^1\text{O}_2$ production, 1H-phenalen-1-one (PN), included in the same xerogel. The trend between their

ability to oxidize organic pollutants in the gas phase and their efficiency for $^1\text{O}_2$ production is investigated through photooxidation experiments of a test pollutant dimethylsulfide (DMS). The Φ_{Δ} value is high for DCA-SG relative to the PN reference, whereas it is slightly lower for 4BB-SG and for ANT-SG. Φ_{Δ} is related to the production of sulfoxide and sulfone as the main oxidation products for DMS photosensitized oxidation. Additional mechanisms, leading to C–S bond cleavage, appear to mainly occur for the less efficient singlet oxygen sensitizers 4BB-SG and ANT-SG.

1. Introduction

For several decades, considerable interest has focused on the first excited electronic state of molecular oxygen [O_2 ($^1\Delta_g$)], denoted below as $^1\text{O}_2$.^[1] This species is recognized as an important oxidizing intermediate in chemical as well as in biological processes. This powerful oxidant is involved in photosensitized processes^[2,3] and has been the subject of many investigations for applications in synthesis,^[4] photodegradation,^[5] phototherapy,^[6] and phototoxicology.^[7] Although several non-photochemical routes exist for the generation of $^1\text{O}_2$, photosensitization is the most commonly employed method in solution and is also primarily responsible for its production in vivo.^[8] The interaction between ground-state molecular oxygen and a large number of excited organic molecules (e.g. aromatic hydrocarbons and ketones, xanthene dyes, pigments such as porphyrins, chlorophylls, flavins, and metal complexes) leads to the production of $^1\text{O}_2$ by energy transfer. Many studies provide evidence of $^1\text{O}_2$ photosensitized generation in a large variety of solvents,^[9] as well as in microheterogeneous systems.^[10,11]

It is important to note that the $^1\text{O}_2$ lifetime varies considerably depending on its environment^[12–14] and that the nature of the media may also affect the quantum yields of $^1\text{O}_2$ production.^[15] While the determination of the quantum yields of $^1\text{O}_2$ production (Φ_{Δ}) is well established in homogeneous systems (usually using a well-known sensitizer as a reference), few studies have dealt with this determination in heterogeneous systems (liquid/solid, gas/solid). Although oxygen quenching of photoexcited species on silica gels^[16–18] has been reported and the generation of $^1\text{O}_2$ is well established, detailed results concerning lifetimes and quantum yields of this reactive oxygen

species (ROS) in gas/solid systems are scarce or unknown. From an application point of view, the production of $^1\text{O}_2$ using a solid system (sensitizer supported on a solid matrix) can be advantageous, especially for the separation of the sensitizer from the reaction medium and recycling purposes. A recent paper by S. Jockush et al.^[19] describes the time-resolved detection of $^1\text{O}_2$ phosphorescence in the near infrared (NIR, 1270 nm)^[20] for determining $^1\text{O}_2$ lifetimes in Y-zeolites [$\text{Na}_x\text{-(AlO}_2)_y\text{(SiO}_2)_z$] and porous silica. To the best of our knowledge, this is the first determination of $^1\text{O}_2$ lifetime in zeolites by time-resolved phosphorescence. Two zeolites with different Si/Al ratios were used: Zeolyst CBV 100 and Zeolyst CBV 901 with an Si/Al ratio of 2.4 and 80, respectively. Both consisted of accessible supercages (diameter about 13 Å) and entry windows of 8 Å. The silica material was 80% microporous (40 Å) and 20% mesoporous (120 Å). Using benzophenone as a sensitizer, the authors showed that the lifetime of $^1\text{O}_2$ decreases with the Si/Al ratio (35 μs for CBV 901 and 7.9 μs for CBV 100). An even

[a] Dr. C. Cantau, Dr. T. Pigot, Dr. S. Lacombe
IPREM-ECP, UMR CNRS 5254
2 rue Pst. Angot, 64053 Pau Cédex 9 (France)
Fax: (+33) 559-407-451
E-mail: sylvie.lacombe@univ-pau.fr

[b] Dr. N. Manoj, Dr. E. Oliveros[†]
Lehrstuhl für Umweltmesstechnik, Engler Bunte Institut
Universitaet Karlsruhe, 76128 Karlsruhe (Germany)

[[†]] Current address:
Laboratoire des IMRCP-UMR CNRS 5623
Université Paul Sabatier, 118 route de Narbonne
F-31062 Toulouse Cédex 9 (France)

longer $^1\text{O}_2$ lifetime was observed in the silica material (64 μs), consistent with $^1\text{O}_2$ quenching by alumina anions. Previously, in 1990, Lu and Thomas^[10] obtained lower values of $^1\text{O}_2$ lifetime in a silica gel/cyclohexane system (13.4–21.5 μs depending on the silica gel used). These lifetimes were shorter than the lifetime in pure cyclohexane (24.0 \pm 0.5 μs), and the authors attributed this drop to quenching of $^1\text{O}_2$ by hydroxyl groups (e.g. adsorbed water and silanol groups) on the silica surface. To account for their relative higher $^1\text{O}_2$ lifetime in porous silica, S. Jockush et al.^[19] insisted on the fact that all their samples were dried under vacuum (10^{-5} Torr) for two hours prior to measurements. The increase of the $^1\text{O}_2$ lifetime was thus due to solvents and water removal. The quenching role of water was illustrated by studying the zeolite samples after addition of 20% water.

Hydroxyl groups are known to deactivate $^1\text{O}_2$ very efficiently.^[21,22] S. Jockush et al. also investigated the influence of the sensitizer on the $^1\text{O}_2$ lifetime by loading zeolite samples with different sensitizers, such as xanthone, thioxanthone and thionine. The lifetimes obtained were slightly shorter than with benzophenone, indicating that $^1\text{O}_2$ was quenched by the sensitizer. Very recently, D. E. Wetzler et al.^[23] measured the quantum yields of $^1\text{O}_2$ production (Φ_{Δ}) in an air-equilibrated solid phase for the first time. They used methylene blue (MB), a well-known $^1\text{O}_2$ sensitizer, supported in Nafion-Na films and compared $^1\text{O}_2$ generation in the air/solid system, in methanol solution and in methanol-swollen Nafion films. The experiments were performed by monitoring the time-resolved $^1\text{O}_2$ emission at 1270 nm. Integration of the $^1\text{O}_2$ emission decay led to the determination of the $^1\text{O}_2$ lifetime (10–90 μs depending on the conditions) and of Φ_{Δ} values (0.24 and 0.47 relative to the reference compound [Ru(bpy)₃]²⁺ in acetonitrile solution). The evaluation of the dependence of the $^1\text{O}_2$ lifetime and of the quantum yields of $^1\text{O}_2$ production on its environment (type of sensitizer, water or solvent content, nature of the solid support) thus appears as an interesting challenge.

One of the potential applications of these supported sensitizers is the photodegradation of undesirable compounds in heterogeneous liquid–solid^[24,25] or gas–solid systems.^[26–28] The aim of our work was to evaluate the quantum yields of $^1\text{O}_2$ production by different silica-supported sensitizers (PS), to determine the $^1\text{O}_2$ lifetime in these systems and to look for a trend between their ability to oxidize organic pollutants in the gas phase and their efficiency for $^1\text{O}_2$ production. Different photosensitizers (Figure 1) were encapsulated in silica monoliths in parallelepiped form, elaborated by a sol–gel process.^[26] These sensitizers (PS) were chosen according to their well-known photooxidation properties in solution^[29] or in the gas phase.^[26–28] For the purpose of comparison, photooxidation experiments of dimethylsulfide (DMS), chosen as a test pollutant in gaseous effluents, were carried out.

Experimental Section

Preparation of Photosensitizer-Based Silica Monoliths: The silica samples were elaborated by a sol–gel method already described.^[26] Tetramethoxysilane (Aldrich) was chosen as silica alkoxide, metha-

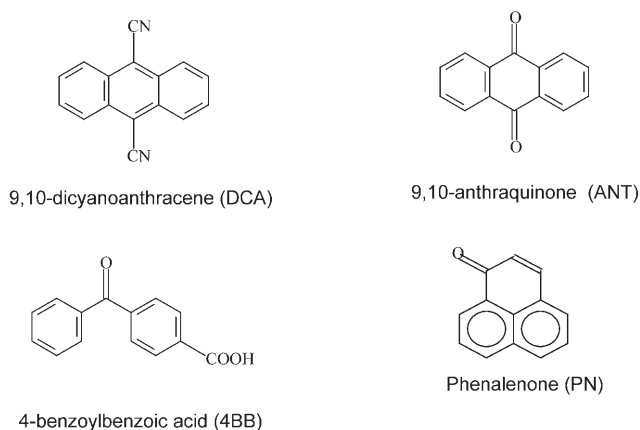


Figure 1. Aromatic molecules used as photosensitizers (PS) in this study.

nol (Fisher, HPLC fluorescence grade) as a corresponding solvent in which the sensitizer (PS) was dissolved, and distilled water as a hydrolysis reaction initiator. The PS used were 9,10-dicyanoanthracene (DCA) (Kodak), 9,10-anthraquinone (ANT) (Acros), 4-benzoylbenzoate acid (4BB) (Acros), and 1*H*-phenalen-1-one (perinaphthone, PN) (Acros). PN was used as a reference sensitizer because it is a well-known and efficient $^1\text{O}_2$ sensitizer ($\Phi_{\Delta} \approx 0.98$ in most solvents).^[30] As the $^1\text{O}_2$ detection system needed a right-angle geometry, the first issue was to obtain monoliths with good mechanical properties and resistance to the laser beam in parallelepiped form with a square side length of at least 5 mm. The choice of the mould for the xerogel was thus crucial. The sol (about 4 mL) was poured into 1 cm long cell (polystyrene cells). After gelification and shrinkage steps, transparent parallelepiped monoliths (5 mm \times 5 mm square basis, 15 mm height) were obtained. In the following, the monoliths are named DCA-SG, ANT-SG, 4BB-SG or PN-SG, depending on the nature of the included sensitizer.

Controlling the absorbance of these samples was another main difficulty of this study. For each sensitizer, three series of monoliths with different absorbances (0.15–0.35) were prepared by varying the sensitizer concentration in the methanol solution used for the sol preparation. The absorption spectra of the monoliths were recorded on a Varian Cary 5 spectrometer and their absorbance was determined at 355 nm.

Nitrogen adsorption and desorption isotherms of the materials were measured at 77 K on a Micromeritics ASAP 2010 Micropore nitrogen adsorption apparatus.

Singlet Oxygen Detection: Singlet oxygen was detected by its weak phosphorescence emission centered at approximately 1270 nm, under both time-resolved and continuous excitation of the PS.

Time-Resolved Phosphorescence Detection (TRPD): Time-resolved detection techniques (TRPD) have been extensively used for the identification of $^1\text{O}_2$, for the determination of $^1\text{O}_2$ lifetimes (τ_{Δ}) in various media and of rate constants of $^1\text{O}_2$ quenching by a large number of substrates and for the measurement of quantum yields of $^1\text{O}_2$ production in photosensitized processes (Φ_{Δ}). The most commonly used method to obtain these values was well described by S. Nonell et al.^[20]

The main features of the time-resolved set-up used in this work for $^1\text{O}_2$ phosphorescence detection (TRPD)^[11] is briefly described below.

A Nd-YAG laser [Continuum Surelite II] equipped with a frequency tripler (355 nm) was used to irradiate the monoliths. The diame-

ter of the beam on the monolith was reduced to approximately 0.3 cm. The energy of the laser pulse was varied between 280 and 1180 μJ using neutral-density filters. Part of the incident beam was deflected using a beam splitter, and an energy meter (Gentec ED-100A) was employed to monitor the energy of the laser pulse. The sample holder usually used in this set-up was designed for standard fluorescence cells as the majority of studies deal with $^1\text{O}_2$ production in solution. For the analysis of the $^1\text{O}_2$ emission in our silica monoliths, a new adapted sample holder was custom-built. The $^1\text{O}_2$ phosphorescence signal was detected in a right-angle geometry with the help of an already described custom-built detector equipped with an InGaAs photodiode (IR Components) and working at room temperature.^[31]

Besides appropriate lenses, the focusing optics included also a cut-off filter at 1098 nm and an interference filter at 1270 nm. The output of the detector was fed to a Tektronix 520A transient recorder and transferred to a personal computer (PC) for storage and kinetic analysis. Typically the laser was run at 1 Hz and 60 shots were averaged for each kinetic trace. It was verified by absorbance measurements at the end of the experiment that no photobleaching of the PS occurred under these conditions.

Steady-State Phosphorescence Detection (SSPD): The custom-built equipment used to monitor the $^1\text{O}_2$ luminescence at 1270 nm upon continuous monochromatic excitation of a sensitizer has already been described.^[32]

For the experiments reported in this article, a cooled (-80°C) NIR photomultiplier (Hamamatsu) was used as a $^1\text{O}_2$ detector, instead of a Ge photodiode. The monoliths were irradiated at 355 nm with a xenon/mercury arc (1 kW) through a water filter, focusing optics, and a monochromator. The $^1\text{O}_2$ luminescence was collected with a mirror, chopped (at 11 Hz) and, after passing through a focusing lens, a cut-off filter (1000 nm) and an interference filter (1271 nm), was detected at 90° with respect to the incident beam using the NIR photomultiplier. Singlet oxygen luminescence signals were recorded as a function of irradiation time during approximately three minutes and no sensitizer bleaching in the monoliths was observed during irradiation.

Photodegradation Experiments: Sensitized photooxidation of gaseous dimethylsulfide (DMS) (Aldrich) was carried out with each PS/silica system by irradiation at 350 nm of a cylindrical reactor containing the grounded materials and located inside a Rayonet device, fitted with 15 RPR-3500 lamps. The scheme of the single-path flow reactor used for the gas-phase photooxidation experiments has already been described.^[26] The gas outlet was directly sampled by a pneumatic valve located on the injection port of a VARIAN 3800 chromatograph equipped with a Chrompack column CPSil-5CB (30 m, 0.25 mm, $1\ \mu\text{m}$). The gas flow was analyzed every 10 min and the concentration of pollutant or of its oxidation products was thus followed over the whole experiment, after identification of the oxidation products by comparison with pure standards or analysis by gas chromatography mass spectrometry (GC-MS). Alternatively, a Varian CP-4900 micro-GC with a thermal conductivity detector could be used to detect sulfur dioxide, carbon dioxide or water in the effluent. These experiments were thus carried out under continuous gas flow, and the breakthrough curve of DMS (i.e. the concentration of DMS in the effluent against time) could be determined both in the dark (adsorption step) and under irradiation (photooxidation step). The percentage abatement of DMS was calculated as the ratio of removed DMS (deduced from the integration of its breakthrough curve under irradiation) to the total entering flow of DMS.

During irradiation, the components of the gas flow could eventually be concentrated on a Carboxen solid-phase microextraction (SPME) fiber, which was then desorbed in the injector of a HP 5973 GC-MS chromatograph (column SPB35, 60 m, 0.32 mm, $1\ \mu\text{m}$) for analysis and identification of the unknown oxidation products. Finally, the materials after irradiation were separated in two sets: the first was sonicated for 30 min in dichloromethane, and the second in deionized water. The dichloromethane solution was analysed by GC for identification and quantification of desorbed organic products. The aqueous extract was analyzed by ion exchange chromatography (IEC) in the suppressed conductivity mode on a Dionex DX-20 chromatograph equipped with an AS9-HC (4 mm) column to identify acidic compounds. Total organic carbon (TOC) was also determined (with a Shimadzu total organic carbon analyzer) on these aqueous extracts in order to quantify all the water-soluble inorganic and organic compounds.

2. Results

2.1. Characterization of the Materials

Silica monoliths in a parallelepiped shape ($5 \times 5 \times 15\ \text{mm}$) were prepared by a sol-gel process according to the procedure described in the Experimental Section. Their specific surface area was $750\ \text{m}^2\text{g}^{-1}$, with an adsorption isotherm characteristic of a microporous material with 21% of mesoporous surface (Figure 2). These data do not depend on the structure of the photosensitizer (PS), or on its concentration in the used range.

Varying amounts of the $^1\text{O}_2$ sensitizer were encapsulated in the monoliths so that final absorbances between 0.15 and 0.35 at the wavelength of excitation (355 nm) were obtained. The amount of PS in the MeOH solution to obtain silica monoliths with the required absorbance had to be determined before their preparation. It should be noted that the PS concentration in the silica xerogel required to reach a given absorbance value depended considerably on the nature of the PS, due to the large variation of the molar absorption coefficients at 355 nm. The different values of absorbance obtained for each series of monoliths containing 9,10-dicyanoanthracene (DCA-SG), 9,10-anthraquinone (ANT-SG), 4-benzoyl benzoate (4BB-SG) or the reference sensitizer 1*H*-phenalen-1-one (PN-SG), are listed in Table 1. In the case of ANT, the values of absorbance

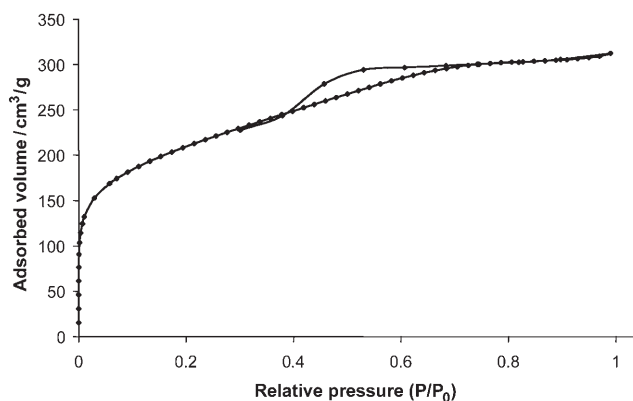


Figure 2. N_2 adsorption and desorption isotherms of a parallelepiped sol-gel monolith at 77 K.

Table 1. Photosensitizer concentrations and absorbances at 355 nm for the monoliths used herein.			
Photosensitizer (PS)	Sample name	PS concentration [mol g ⁻¹]	Absorbance at 355 nm
PN	PN-SGmin	$(4.5 \pm 0.2) \times 10^{-8}$	0.18 ± 0.02
	PN-SGmed	$(5.7 \pm 0.2) \times 10^{-8}$	0.21 ± 0.02
	PN-SGmax	$(7.2 \pm 0.3) \times 10^{-8}$	0.25 ± 0.02
DCA	DCA-SGmin	$(1.22 \pm 0.03) \times 10^{-7}$	0.19 ± 0.01
	DCA-SGmed	$(1.51 \pm 0.03) \times 10^{-7}$	0.26 ± 0.02
	DCA-SGmax	$(1.82 \pm 0.04) \times 10^{-7}$	0.31 ± 0.02
ANT	ANT-SGmin	$(5.2 \pm 0.1) \times 10^{-7}$	0.40 ± 0.02
	ANT-SGmed	$(8.6 \pm 0.2) \times 10^{-7}$	0.60 ± 0.02
	ANT-SGmax	$(1.03 \pm 0.03) \times 10^{-6}$	0.80 ± 0.02
4BB	4BB-SGmin	$(4.3 \pm 0.1) \times 10^{-6}$	0.18 ± 0.02
	4BB-SGmed	$(5.4 \pm 0.1) \times 10^{-6}$	0.20 ± 0.02
	4BB-SGmed-2	$(7.4 \pm 0.1) \times 10^{-6}$	0.28 ± 0.02
	4BB-SGmax	$(1.08 \pm 0.03) \times 10^{-5}$	0.38 ± 0.02

were higher than expected, as ANT displays a broad absorption band between 300 and 380 nm with a steep slope at 355 nm (Figure 3). Hence, the accurate concentration needed

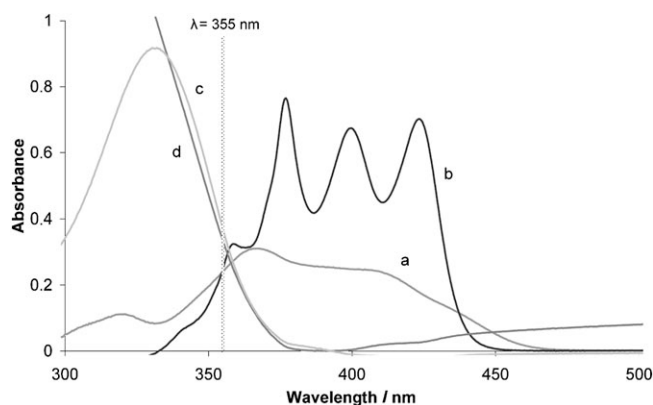


Figure 3. Absorbance spectra (300–500 nm) of sensitizer-doped parallelepiped sol-gel monoliths: a) PN-SGmax, [PN] = $(7.2 \pm 0.3) \times 10^{-8}$ mol g⁻¹; b) DCA-SGmed, [DCA] = $(1.51 \pm 0.03) \times 10^{-7}$ mol g⁻¹; c) ANT-SGmin, [ANT] = $(5.2 \pm 0.1) \times 10^{-7}$ mol g⁻¹; d) 4BB-SGmax, [4BB] = $(1.08 \pm 0.03) \times 10^{-5}$ mol g⁻¹.

to achieve the required absorbance was more difficult to evaluate. The absorbance spectra of the monoliths are given in Figure 3.

2.2. Singlet Oxygen Lifetimes in the Monoliths

Singlet oxygen lifetimes (τ_{Δ}) in the monoliths were determined by time-resolved phosphorescence detection (TRPD, Experimental Section). Typical signals obtained with the ANT/silica

system (ANT-SGmed, Table 1) are presented in Figure 4a. The ¹O₂ phosphorescence decay traces observed for all the monoliths could be fitted with single exponential functions from which τ_{Δ} values could be derived [Eq. (1), Table 2].

$$S_t = S_0 \exp(-t/\tau_{\Delta}), \quad (1)$$

where S_t and S_0 are the amplitudes of the ¹O₂ luminescence signals at time t and extrapolated at zero time (laser pulse), respectively.

Values of τ_{Δ} were found to vary between 22 and 25 μ s, except for 4BB monoliths in which ¹O₂ had a shorter lifetime (≈ 17.0 μ s). This could be the consequence of ¹O₂ quenching by either an impurity inside the monolith or by 4BB itself (see the Discussion). As expected, signals of increasing intensity were observed as the laser excitation energy increased (Figure 4b), but τ_{Δ} values were not affected (within experimental error) in the PS concentration ranges investigated.

2.3. Quantum Yields of Singlet Oxygen Production in the Monoliths

2.3.1. Time-Resolved Measurements

The determination of the quantum yields of ¹O₂ production (Φ_{Δ}) in the monoliths was also based on the detection of the ¹O₂ luminescence. This technique involves relative measurements and requires the use of a reference sensitizer of known Φ_{Δ} (Φ_{Δ}^R), both under time-resolved and steady-state conditions. In this work, monoliths containing phenalene (PN-SG) were employed as a reference, since PN exhibits a Φ_{Δ} close to unity (this value is practically insensitive to the medium), and is widely used as a standard ¹O₂ sensitizer.^[30] Therefore, we have assumed in the following that the quantum yield for phenalene is not significantly modified in the solid medium.

In the time-resolved regime (Experimental Section), Φ_{Δ} values were determined by two methods. In method (a), the zero-time intensity (S_0) of the decay signals was measured as a function of the laser energy for monoliths containing the dif-

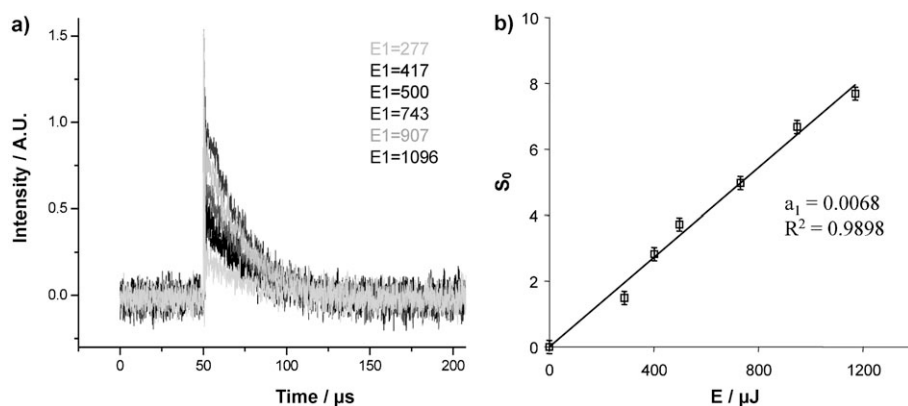


Figure 4. a) Singlet oxygen luminescence decay signals at 1270 nm for the monolith ANT-SGmed (Table 1) excited at 355 nm as a function of the laser excitation energy (E_i in μ J); b) zero-time amplitude S_0 as a function of the laser energy.

PS-SG	$^1\text{O}_2$ lifetime, τ_Δ [μs]	Quantum yields of $^1\text{O}_2$ production (Φ_Δ)		
		Time-resolved singlet oxygen detection (S_0) ^[a]	Time-resolved singlet oxygen detection (area) ^[b]	Steady-state measurements ^[c]
PN-SG	24.7 ± 0.5	1.0	1.0	1.0
DCA-SG	22.5 ± 0.7	1.1 ± 0.1	1.0 ± 0.1	1.2 ± 0.1
ANT-SG	23 ± 1	0.8 ± 0.1	0.8 ± 0.1	0.8 ± 0.1
4BB-SG	17.0 ± 0.9	-	0.9 ± 0.1	0.9 ± 0.1

[a] Time-resolved near-infrared detection using S_0 values; [b] time-resolved near-infrared detection by integration of the emission signal (area); [c] steady-state measurements.

ferent sensitizers (PS-SG) and the reference (PN-SG) at various absorbances (Table 1). S_0 is related to Φ_Δ according to Equation (2) (see, for example, ref. [20]),

$$S_0 = KE_1 (1 - 10^{-A}) \Phi_\Delta, \quad (2)$$

where K is a proportionality factor which includes geometric and electronic factors of the detection system as well as characteristics of the medium (refractive index, NIR absorption) and the $^1\text{O}_2$ radiative rate constant (solvent dependent), E_1 is the energy of the laser pulse, and A the absorbance of the monolith at the wavelength of excitation (355 nm); the product E_1

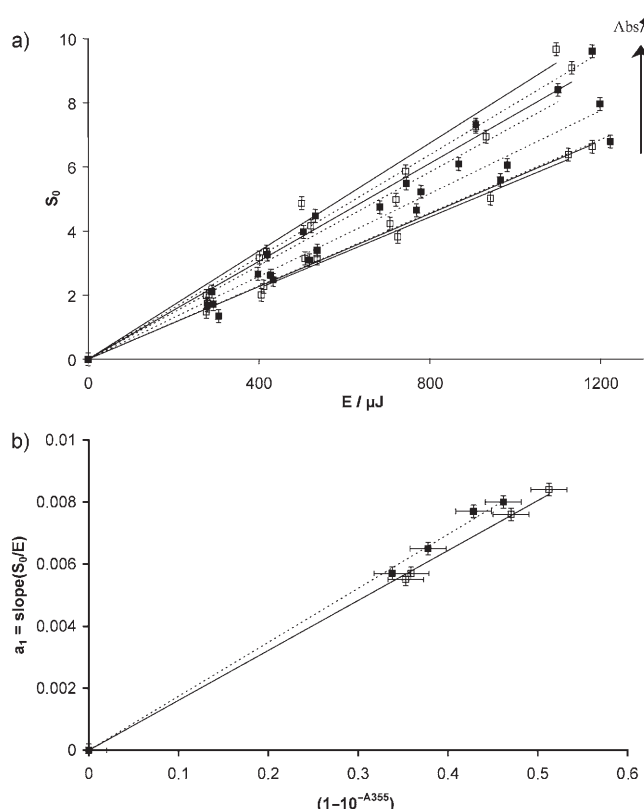


Figure 5. a) Zero-time amplitude S_0 as a function of laser energy for a set of ANT-SG (\square) and reference PN-SG (\blacksquare) monoliths with different absorbance values with excitation at 355 nm. b) Slopes of laser energy-dependent slopes a_1 (from a) as a function of the absorption factor $(1 - 10^{-A})$ for ANT-SG (\square) and PN-SG (\blacksquare).

$(1 - 10^{-A})$ represents therefore the energy absorbed by the PS-SG during the pulse. The factor K remains constant when all experiments are carried out with the same equipment and in the same medium.

S_0 was measured as a function of the laser energy for the three available monoliths containing a given sensitizer (PS-SG) and the reference monoliths (PN-SG) at different absorbances. The series

of measurements was repeated at least twice for each monolith. The slopes of the straight lines obtained for the variation of S_0 as a function of E_1 [$a_1 = K\Phi_\Delta(1 - 10^{-A})$] were calculated for each PS-SG and PN-SG (Figures 4b and 5a), and plotted against the absorption factor $(1 - 10^{-A})$. The ratio of the slopes a_2 ($K\Phi_\Delta$) thus obtained is the same as the Φ_Δ ratio between PS-SG and PN-SG [Eq. (3)]. It should be noted that observation of linearity with zero intercept rules out any unwanted phenomenon such as multiphotonic absorption or saturation of the triplet excited state of the sensitizer.

$$\Phi_\Delta^S / \Phi_\Delta^R = a_2^S / a_2^R \quad (3)$$

where the superscripts "S" and "R" stand for monoliths PS-SG and PN-SG (reference), respectively.

The second method (b) relied on the integration of the area below the time-resolved $^1\text{O}_2$ emission signal, instead of using the value of S_0 . The integrated area (IA) depends on the same factors as S_0 [Eq. (2)] but also on τ_Δ [Eq. (4)]:

$$IA = KE_1 (1 - 10^{-A}) \Phi_\Delta \tau_\Delta \quad (4)$$

The same procedure as described above for method (a) was followed for IA . In this case, the slopes a_2' are equal to $K\Phi_\Delta\tau_\Delta$ and show the same ratio as the products $\Phi_\Delta\tau_\Delta$ for PS-SG and PN-SG. Therefore, Φ_Δ values for the PS-SG monoliths were calculated using Equation (5):

$$\Phi_\Delta^S / \Phi_\Delta^R = (a_2'^S / a_2'^R) (\tau_\Delta^R / \tau_\Delta^S) \quad (5)$$

2.3.2. Steady-State Measurements

Quantum yields of $^1\text{O}_2$ production were also determined under continuous irradiation of the monoliths (steady-state measurements, Experimental Section). This method was of particular interest as sensitized photooxidations of model pollutants are carried out under continuous irradiation (Experimental Section).^[26–28] The relation between the intensity of the $^1\text{O}_2$ luminescence signal (S_{ss}) and Φ_Δ [Eq. (6)] is similar to that given in Equation (4).

$$S_{ss} = K'P_0(1 - 10^{-A})\Phi_\Delta\tau_\Delta \quad (6)$$

where P_0 is the incident photon flux received by the monolith from the continuous irradiation source at the wavelength of excitation (selected by a monochromator, Experimental Section).

Square signals were obtained showing that the sensitizers in the monoliths were stable under continuous irradiation (Figure 6). Similarly to the time-resolved experiments, the intensity of the signal (S_s) was plotted as a function of the absorption factor ($1-10^{-A}$). The slope $a_3 (=K'P_0\Phi_{\Delta}\tau_{\Delta})$ was calculated. The ratio of the slope a_3 obtained for each PS-SG and for PN-SG allowed the determination of the quantum yield of $^1\text{O}_2$ production for each PS-SG, using Equation (7).

$$\Phi_{\Delta}^S/\Phi_{\Delta}^R = (a_3^S/a_3^R)(\tau_{\Delta}^R/\tau_{\Delta}^S) \quad (7)$$

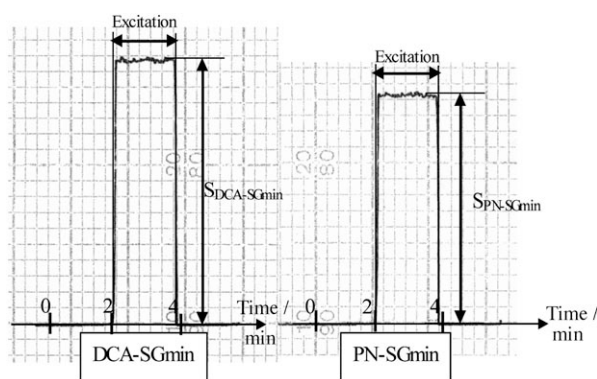


Figure 6. Singlet oxygen luminescence signals from two monoliths, DCA-SGmin and PN-SGmin, under continuous excitation at 355 nm.

Whatever the method used for their determination, the values of the quantum yields of $^1\text{O}_2$ production (relative to the PN standard, Table 2) were high (≥ 0.8), indicating that the PS-SG monoliths were good $^1\text{O}_2$ sensitizers. The values obtained with the different methods were found to be similar within experimental error and appeared to be consistent, except in the case of 4BB with method (a), time-resolved measurements using the zero-time amplitude of the $^1\text{O}_2$ signal (S_0). The value of Φ_{Δ} for 4BB-SG determined by this method was much higher than with the other methods and appeared unreliable (probably due to errors in the extrapolation of the signal at zero time). The determined quantum yields were found in the order $\Phi_{\Delta}(\text{DCA}) > \Phi_{\Delta}(\text{4BB}) > \Phi_{\Delta}(\text{ANT})$, with a value for $\Phi_{\Delta}(\text{DCA})$ very close to that of the PN standard. DCA is thus at least as good a sensitizer in silica monoliths as PN.

2.4. Photodegradation Experiments

Before testing the photocatalytic efficiency of each PS encapsulated in silica xerogel monoliths at the gas–solid interface, a previous adsorption step of the pollutant was performed to achieve saturation of the material. The operating conditions [catalyst mass, gas flow, inlet dimethylsulfide (DMS) concentration, absence of humidity, irradiation time, and wavelengths] were identical for all the samples to compare the PS efficiency for DMS removal and to draw some conclusions on the involved mechanisms.

The efficiency of the material, that is, DMS consumption, was evaluated from the percent abatement calculated as the ratio of removed DMS (deduced from the integration of its breakthrough curve under irradiation) to the total entering flow of DMS. The initial DMS removal rate was also determined from the slope of the curve at the beginning of the irradiation. The results are summarized in Table 3.

The reactor was loosely packed with 0.6 g of pieces of monoliths previously broken open. The volume taken up by the material in the reactor was the same and hence the value of the gas hourly sample velocity (GHSV, h^{-1})^[33] was identical in all experiments. For the purpose of comparison, all the experiments were carried out for the same irradiation time (120 h). To compare with singlet oxygen measurements, all irradiations were carried out at 350 nm (15 RPR-3500 lamps). If possible, monoliths with different PS were chosen in order to present the same absorbance at 350 nm, close to 0.25–0.28. This condition was difficult to hold with ANT-SG ($\text{Abs} \approx 0.40$), due to the sharp slope of the absorption spectrum at 350 nm (Figure 3). Under these conditions, DCA-SG (entry 2, Table 3) showed the best activity for DMS abatement (80%) with one of the highest DMS removal initial rate (-4.5 ppmv h^{-1}). For PN-SG (entry 1, Table 3), ANT-SG (entry 3, Table 3) and 4BB-SG (entry 4, Table 3), the DMS removal initial rate were similar, around 3 ppmv h^{-1} , and lower than that observed with DCA-based material. Nevertheless, the DMS abatement was not the same for these three latter materials. Indeed, DMS abatement decreased in the order PN-SG (55%) > ANT-SG (47%) > 4BB-SG (32%).

Organic and inorganic products, detected in the gas phase at the outlet of the reactor or adsorbed on the materials after irradiation, are reported in Table 4. Under these operating conditions, no CO_2 or H_2O was detected in the gas phase with any of these materials. With DCA-SG, the compounds detected in the gas phase represented 26.5%, with DMS as the main observed compound (26.0%), together with traces of dimethylsulfoxide (DMSO) and dimethyldisulfide (DMDS). Organic prod-

Table 3. Efficiency of DMS removal for each photocatalyst under identical conditions after 120 h of irradiation (0.6 g of PS-SG, flow-rate: 67 mL mn^{-1} , GHSV = 2250 h^{-1} , inlet DMS concentration: 100 ppmv, irradiation at 350 nm).

Entry	Photocatalyst used	Absorbance at 355 nm	PS concentration [mol g^{-1}]	DMS removal initial rate [ppmv h^{-1}]	DMS abatement [%]
1	PN-SGmax	0.25 ± 0.02	9.9×10^{-8}	-3.0	55
2	DCA-SGmed	0.26 ± 0.02	8.3×10^{-8}	-4.5	80
3	ANT-SGmin	0.40 ± 0.02	2.8×10^{-7}	-3.0	47
4	4BB-SGmed-2	0.28 ± 0.02	4.1×10^{-6}	-2.9	32

ucts extracted from the material by washing in CH_2Cl_2 were analyzed by GC-FID. Mainly DMSO (26.8%) and DMSO_2 (22.3%) were observed. In the water extract analysed by ion exchange chromatography (IEC), only traces of acids were detected ($\approx 0.9\%$).

Highly polar DMSO and DMSO_2 interact strongly with silica xerogel and hence accumulated on these materials. These strongly adsorbed products were probably not efficiently desorbed, which accounts for the slightly lower material balance in this case (77.5% of the introduced DMS amount). Moreover, another point of concern for this low material balance is the impossible DMS quantification in the organic extract due to overlapping with solvent chromatographic peak. It was thus verified that only low DMS amounts were desorbed at 30 and 100 °C from the irradiated DCA-SG in a headspace thermodesorber coupled with a GC-MS. Hence, unreacted DMS cannot account for this low material balance.

Concerning ANT-SG and 4BB-SG, DMS was mainly detected in the gas phase (55.0 and 65.3%, respectively, of introduced DMS). Low amounts of DMDS (3.5 and 5.4% respectively) were also observed, the main difference being the detection of traces of DMSO with 4BB-SG. The analysis of the organic extract confirmed the formation of DMDS (0.7% for ANT-SG and 0.5% for 4BB-SG), and also of DMSO (20.7 and 12.1% respectively), DMSO_2 (6.6 and 3.1%, respectively) and methyl methanethiosulfonate (MMTS, $\text{H}_3\text{C}-\text{S}(\text{O})_2-\text{S}-\text{CH}_3$) (0.6 and 1.2%, respectively), as for DCA but in lower amounts. This is in agreement with a lower DMS removal with ANT-SG and 4BB-SG. Several acids (6.2 and 8.3%, respectively), mainly formate (1.4 and 1.8%), sulfinate (3.6 and 3.5%), sulfonate (1 and 2.8%), and sul-

fate (0.2% in both cases), were detected in the water extract. In both cases, the material balance (93.4 and 96%, respectively, with ANT-SG and 4BB-SG) was higher than with DCA-SG, which may be related to a lower DMS abatement and to the less selective formation of highly polar compounds, such as sulfoxide and sulfone, hardly desorbed from the materials.

To better understand the photooxidation mechanisms, it was interesting to perform the same study with PN-SG, as PN is a pure singlet oxygen sensitizer. DMS was the main compound detected in the gas phase (44.7% of introduced DMS). Nevertheless, we also observed low amounts of DMDS (0.2%). Only traces of acids and large amounts of DMSO and DMSO_2 were observed after desorption of the material and confirmed the predominance of a mechanism involving $^1\text{O}_2$ addition.

In summary, although less efficient, ANT-SG and 4BB-SG produced more acids, along with DMSO and DMSO_2 , significant amounts of DMDS and traces of MMTS and dithiapentane, while in the cases of PN-SG and DCA-SG, DMSO and DMSO_2 were almost the only products detected.

3. Discussion

As demonstrated by time-resolved and steady-state analysis of the $^1\text{O}_2$ phosphorescence, 9,10-dicyanoanthracene ($\Phi_{\Delta} \approx 1.1$), 9,10-anthraquinone ($\Phi_{\Delta} \approx 0.8$), and 4-benzoylbenzoic acid ($\Phi_{\Delta} \approx 0.9$) are very efficient $^1\text{O}_2$ sensitizers in the silica monoliths. The lifetime of $^1\text{O}_2$ in these systems is of the same order of magnitude when DCA, ANT or the standard PN are used as sensitizers ($\tau_{\Delta} \approx 23\text{--}25 \mu\text{s}$). For 4BB however, a shorter lifetime was measured ($\tau_{\Delta} = 17.0 \pm 0.9 \mu\text{s}$). This result could tentatively

Table 4. Organic products detected in the gas phase and by desorption of the irradiated materials in CH_2Cl_2 and in water (bold characters: yield relative to the initial DMS amount).

	PN-SGmax	DCA-SGmed	ANT-SGmin	4BB-SGmed-2
compounds detected in the gas phase under irradiation ^[a]	44.9%	26.5%	58.5%	70.8%
	DMS (44.7%) DMDS (0.2%)	DMS (26.0%) DMDS (0.2%) DMSO (0.3%)	DMS (55.0%) DMDS (3.5%)	DMS (65.3%) DMDS (5.4%) DMSO (0.1%)
compounds desorbed from the material after irradiation	37.8%	50.1%	28.7%	16.9%
% products desorbed in CH_2Cl_2 ^[b]	DMSO (21.4%) DMSO_2 (16.2%) MMTS (0.2%) traces of DMDS and dithiapentane	DMSO (26.8%) DMSO_2 (22.3%) MMTS (1%) traces of DMDS and dithiapentane	DMSO (20.7%) DMSO_2 (6.6%) MMTS (0.6%) DMDS (0.7%) dithiapentane (0.1%)	DMSO (12.1%) DMSO_2 (3.1%) MMTS (1.2%) DMDS (0.5%) dithiapentane (traces)
% products desorbed in water ^[c]	0.4%	0.9%	6.2%	8.3%
	sulfinate (0.2%) formate (0.1%) sulfonate (0.1%) sulfate (traces)	sulfinate (0.3%) formate (0.4%) sulfonate (0.2%) sulfate (traces)	sulfinate (3.6%) formate (1.4%) sulfonate (1.0%) sulfate (0.2%)	sulfinate (3.5%) formate (1.8%) sulfonate (2.8%) sulfate (0.2%)
material balance [%]	83	77.5	93.4	96
DMDS: dimethyldisulfure; DMSO: dimethylsulfoxide; DMSO_2 : dimethylsulfone; MMTS: methyl methanethiosulfonate: $\text{CH}_3\text{S}(\text{O})_2\text{SCH}_3$; dithiapentane: $\text{CH}_3\text{SCH}_2\text{SCH}_3$. [a] Quantified by integration on the whole experiment of the DMS and DMDS signals using the inline GC-FID chromatographs. [b] Quantified by GC-FID determination of the organic extract using the internal standard method. [c] Quantified by IEC chromatography determination of the aqueous extract using the external standard method.				

be accounted for by quenching of $^1\text{O}_2$ by impurities inside the xerogel. However, all the synthesized materials were prepared at the same time under identical conditions. Hence, the same undesirable impurities should be present in all the studied monoliths. The other explanation could be $^1\text{O}_2$ quenching by 4BB itself. Bimolecular rate constants of $^1\text{O}_2$ quenching (k_q) by anthracene and benzophenone in benzene solutions have been reported to be $1.6 \times 10^5 \text{ L mol}^{-1} \text{ s}^{-1}$ and $3.0 \times 10^4 \text{ L mol}^{-1} \text{ s}^{-1}$, respectively.^[9] Therefore, anthracene is five times more efficient as a $^1\text{O}_2$ quencher than benzophenone, in apparent contradiction with lifetime measurements. However, the concentrations of the sensitizers in the xerogel monoliths have to be taken into account. To achieve absorbance values in the range 0.15–0.35 in the xerogel monoliths, the required 4BB concentration is about 35 times larger than that of DCA (Table 1), and hence, the quenching of singlet oxygen is seven times more efficient for monoliths with same absorbance at 355 nm [Eq. (8)].

$$\frac{k_{q(4BB)} \cdot [4BB]}{k_{q(DCA)} \cdot [DCA]} \approx 7 \quad (8)$$

Our results on Φ_Δ and τ_Δ may be compared with the scarce literature data found in this field. Jockush et al.^[19] determined the $^1\text{O}_2$ lifetime in silica material with benzophenone as a sensitizer. The τ_Δ value in this system (64 μs) is higher than that measured with our silica xerogel monoliths. It is worth noting that the authors dried their material under high vacuum (10^{-5} Torr) for two hours and hence solvent or residual water were expelled from silica, whereas our monoliths were used without any drying step, except the gelification and shrinking procedure at a maximum temperature of 80 °C under ambient pressure. The presence of methanol and particularly of water can be responsible for the lower $^1\text{O}_2$ lifetimes observed in our samples. In fact, τ_Δ values in these solvents are among the shortest ones (approximately 4 and 12 μs in water and ethanol, respectively^[3,10,11]), shorter than in our monoliths.

Wetzler et al.^[23] quantified the generation of $^1\text{O}_2$ by photosensitization using methylene blue (MB) supported on Nafion®-Na films by TRPD. The quantum yield of $^1\text{O}_2$ production (Φ_Δ) in the air-equilibrated solid phase was determined to be approximately 0.24 relative to $[\text{Ru}(\text{bpy})_3]^{2+}$ in air-equilibrated acetonitrile ($\Phi_\Delta = 0.57$ ^[34]). Since MB and the reference sensitizer ($[\text{Ru}(\text{bpy})_3]^{2+}$) were not dissolved in the same medium, the former being in a solid (Nafion membranes) and the latter in solution, a number of corrections had to be introduced by the authors in order to account for the variation of factor K [Eqs. (2) and (4)], as well as for changes in incident photon fluxes and in absorbances at the excitation wavelengths. In our case, the Φ_Δ of the reference sensitizer (PN) is practically not affected by the medium,^[30] in contrast to $[\text{Ru}(\text{bpy})_3]^{2+}$,^[35] is much higher than that of $[\text{Ru}(\text{bpy})_3]^{2+}$, and all sensitizers were included in the monoliths. Therefore, errors and corrections were minimized.

The quantum yields of singlet oxygen production by DCA, PN, ANT, and benzophenone have been determined in C_6H_6 solution.^[9] The higher value was observed for PN ($\Phi_\Delta = 0.95$),

while lower values are reported for ANT ($\Phi_\Delta = 0.17$) and benzophenone ($\Phi_\Delta = 0.29$). In the case of DCA, there is a large discrepancy in the literature on the Φ_Δ values (ranging from 0.2 to 1.8) depending on the oxygen concentration, the methods of irradiation (continuous vs pulsed) and measurement (chemical versus spectroscopic). Note that Φ_Δ may be higher than 1 for DCA because energy transfer to molecular oxygen can occur not only from the triplet excited state of DCA but also from its singlet excited state.^[36]

Turning now to DMS photooxidation, previous results in solution indicate that both type I (single electron transfer from sulfide) and/or type II (energy transfer to ground-state oxygen leading to singlet oxygen formation) mechanisms are possible with the excited PS used [Eqs. (9) and (10)].^[29]



From the gas-phase photooxidation experiments, DCA-SG (80% DMS abatement) showed the best efficiency relative to PN-SG (55% DMS abatement), ANT-SG (47% DMS abatement), and 4BB-SG (32% DMS abatement).

The highest quantum yields of $^1\text{O}_2$ production ($\Phi_\Delta \approx 1.1$) and longest $^1\text{O}_2$ lifetimes (22.5 μs) were found for DCA-SG relative to PN-SG ($\Phi_\Delta \approx 1.0$ and $\tau_\Delta \approx 24.7 \mu\text{s}$). The former is also found as the most efficient for DMS abatement in the gas phase (Table 3). In both cases, only DMSO and DMSO_2 were detected as byproducts in the gas flow or in the organic extract (Table 4). Their selective formation results from the addition of $^1\text{O}_2$ on dimethylsulfide, as PN-SG is a pure singlet oxygen sensitizer [Eq. (11)].^[37]



The better efficiency on DMS removal initial rate (-4.5 and -3 ppmv h^{-1} , respectively) and DMS abatement (80 and 55%) observed with DCA-SG relative to PN-SG may tentatively be accounted for by a competitive electron transfer mechanism [Eq. (9)], often put forward for DCA photosensitized reactions, and only possible in the presence of DMS.^[38–40] The resulting cleavage of the C–S bond followed by radical pathways may explain the slightly higher amounts of by-products such as MMTS and acids in the case of DCA-SG.

ANT-SG, 4BB-SG gave similar results for DMS removal initial rate (about -3 ppmv h^{-1}), and DMS abatement. As mentioned above, the main point of concern is the products distribution, which is obviously different from that obtained with PN-SG and DCA-SG. These latter results indicate that with both materials, the type I mechanism is probably operative, besides $^1\text{O}_2$ -mediated oxidation: electron transfer mechanisms leading to radical intermediates (arising from initial formation of sulfide radical cation [Eq. (9)] and possibly superoxide anion [Eq. (12)]) probably take a large part in the reaction pathways,^[29] the amount of DMDS is at least 20 times higher, as well as the amounts of acid, than those observed with PN-SG or DCA-SG. As a matter of fact, the formation of superoxide radical anion

has recently been reported with anthraquinones in the presence of different electron donors [Eq. (12)].^[41]



Another conclusion emerging from our results with ANT-SG and 4BB-SG is that the prevalence of the electron transfer mechanism results in less-efficient DMS oxidation (initial rate and/or abatement) than through ${}^1\text{O}_2$ addition as with PN-SG or DCA-SG.

In the case of ANT-SG, it is worthy of note that its absorbance value ($\text{Abs}_{355\text{nm}} \approx 0.4$) is higher than those of the other materials, accounting for its efficiency towards DMS removal despite a weaker quantum yield of ${}^1\text{O}_2$ production.

Finally, when comparing PN-SG, DCA-SG and 4BB-SG with similar absorbances, the determined efficiencies, that is, DMS removal initial rate and percentage DMS abatement, are found in the order DCA-SG > PN-SG > 4BB-SG, consistent with the order of the values of quantum yields of ${}^1\text{O}_2$ production ($\Phi_{\Delta}(\text{DCA}) \approx \Phi_{\Delta}(\text{PN}) > \Phi_{\Delta}(\text{4BB})$). The lower efficiency of 4BB-SG can be probably accounted for by the shorter lifetime of ${}^1\text{O}_2$ in this material (17 μs).

4. Conclusions

To the best of our knowledge, this work reports for the first time quantum yields of ${}^1\text{O}_2$ production and ${}^1\text{O}_2$ lifetimes at the gas–solid interface in silica gel material. These results are complementary to the previous ones published by Wetzler et al.,^[23] obtained on a different solid support (silica gel versus Nafion). Moreover, with our approach, any PS soluble in water or methanol can be included in a silica gel support, and not only cationic PS such as those coated on Nafion. The determined lifetimes in silicagel are also consistent with those measured by Jokusch et al.,^[19] taking into account the presence of residual water and solvent in our monoliths. On the whole, the quantum yield of ${}^1\text{O}_2$ production is excellent for DCA-SG relative to the standard sensitizer PN in the same silicagel, whereas it is slightly lower for 4BB-SG (with a derivative of benzophenone as a sensitizer), and for ANT-SG derived from anthraquinone. The quantum yield of ${}^1\text{O}_2$ production is related to the production of sulfoxide and sulfone as main oxidation products for dimethylsulfide photosensitized oxidation at the gas–solid interface. Additional mechanisms, leading to C–S bond cleavage, appear to occur mainly for the less-efficient singlet oxygen producers 4BB-SG and ANT-SG.

For all the PS-based silicagel investigated, grafting of the photosensitizer on the silica support should increase their stability. Their regeneration by desorption of polar oxidation products in suitable solvents should allow their use for several cycles without decrease of ${}^1\text{O}_2$ production and loss of efficiency.^[28] Such photosensitizing materials, leading to products arising from partial oxidation (to be compared with mineralization), may be used for decontamination purpose, complementing conventional TiO_2 -based photocatalysis, leading to mineralization. Further work aimed at the elaboration of stable material with different grafted photosensitizing molecules is currently

under progress to widen the possible range of applications. Elaboration of hydrophobic silica xerogel will also be investigated to increase ${}^1\text{O}_2$ lifetime by limiting the quenching of ${}^1\text{O}_2$ by residual water or solvent.

Acknowledgements

The authors gratefully acknowledge the financial support of the ADEME for this study and the Centre Technique du Papier for technical collaboration.

Keywords: photooxidation · sensitizer · singlet oxygen · sol-gel processes · time-resolved spectroscopy

- [1] A. P. Schaap, *Singlet Molecular Oxygen*, Dowden, Hutchinson and Ross, Stroudsburg, 1976.
- [2] C. S. Foote in *Free Radicals in Biology*, Vol. 2 (Ed.: W. A. Pryor), Academic, New York, 1976, pp. 85–133.
- [3] C. S. Foote, E. L. Clennan in *Active Oxygen in Chemistry* (Eds.: C. S. Foote, J. S. Valentine, A. Greenberg, J. F. Liebman), Chapman and Hall, London, 1995, pp. 105–140.
- [4] G. C. Vougioukalakis, Y. Angelis, J. Vakros, G. Panagiotou, C. Kordulis, A. Lycourghiotis, M. Orfanopoulos, *Synlett* 2004, 971–974.
- [5] P. R. Ogilby, M. Kristiansen, D. O. Martire, R. D. Scurlock, V. L. Taylor, R. L. Clough, *Adv. Chem. Ser.* 1996, 249, 113–126.
- [6] A. A. Krasnovsky in *Light in Biology and Medicine*, Vol. 2 (Eds.: R. H. Douglas, J. Moan, G. Ronto), Plenum, New York, 1991, pp. 431–451.
- [7] M. M. Mathews-Roth in *The Science of Photomedicine* (Eds.: J. D. Regan, J. A. Parris), Plenum, New York, 1978.
- [8] E. Cadenas, *Annu. Rev. Biochem.* 1989, 58, 79–110.
- [9] F. Wilkinson, W. P. Helman, A. B. Ross, *J. Phys. Chem. Ref. Data* 1993, 22, 113–262.
- [10] K.-K. Lu, J. K. Thomas, *J. Am. Chem. Soc.* 1990, 112, 3319–3325.
- [11] L. A. Martinez, C. G. Martinez, B. B. Klopotek, J. Lang, A. Neuner, A. M. Braun, E. Oliveros, *J. Photochem. Photobiol. B* 2000, 58, 94–107.
- [12] R. Schmidt, *J. Am. Chem. Soc.* 1989, 111, 6983–6987.
- [13] J. Catalan, C. Diaz, L. Barrio, *Chem. Phys.* 2004, 300, 33–39.
- [14] R. Schmidt, *Chem. Phys.* 2004, 304, 315–316.
- [15] C. G. Martinez, A. Neuner, C. Marti, S. Nonell, A. M. Braun, E. Oliveros, *Helv. Chim. Acta* 2003, 86, 384–397.
- [16] E. Wellner, D. Rojanski, M. Ottolenghi, D. Huppert, D. Avnir, *J. Am. Chem. Soc.* 1987, 109, 575–576.
- [17] J. K. Drake, P. Levitz, N. J. Turro, K. S. Nitsche, K. F. Cassidy, *J. Phys. Chem.* 1988, 92, 4680–4684.
- [18] J. K. Drake, P. Levitz, J. Klafter, N. J. Turro, K. S. Nitsche, K. F. Cassidy, *Phys. Rev. Lett.* 1988, 61, 865–868.
- [19] S. Jockush, J. Sivaguru, N. J. Turro, V. Ramamurthy, *Photochem. Photobiol. Sci.* 2005, 4, 403–405.
- [20] S. Nonell, S. E. Braslavsky, *Methods Enzymol.* 2000, 319, 37–49.
- [21] F. Wilkinson, W. P. Helman, A. B. Ross, *J. Phys. Chem. Ref. Data* 1995, 24, 663–1021.
- [22] R. Schmidt, E. Afshari, *Ber. Bunsen-Ges.* 1992, 96, 788–794.
- [23] D. E. Wetzler, D. Garcia-Fresnadillo, G. Orellana, *Phys. Chem. Chem. Phys.* 2006, 8, 2249–2256.
- [24] D. Wöhrle, O. Suvorova, R. Gerdes, O. Bartels, L. Lapok, N. Baziakina, S. Makarov, A. Slodek, *J. Porphyrins Phthalocyanines* 2004, 8, 1020–1041.
- [25] D. Wöhrle, N. Baziakina, O. Suvorova, S. Makarov, V. Kutureva, E. Schupak, G. Schnurpfeil, *J. Porphyrins Phthalocyanines* 2004, 8, 1390–1401.
- [26] V. Latour, T. Pigot, P. Mocho, S. Blanc, S. Lacombe, *Catal. Today* 2005, 101, 359–367.
- [27] C. Cantau, T. Pigot, R. Brown, P. Mocho, M. T. Maurette, F. Benoit-Marqué, S. Lacombe, *Appl. Catal. B* 2006, 65, 77–85.
- [28] C. Cantau, S. Larribau, T. Pigot, M. Simon, M. T. Maurette, S. Lacombe, *Catal. Today* 2007, 122, 27–38.
- [29] V. Latour, T. Pigot, H. Cardy, M. Simon, S. Lacombe, *Photochem. Photobiol. Sci.* 2005, 4, 221–229.

- [30] a) E. Oliveros, P. Suardi-Murasecco, T. Arminian-Saghafi, A. M. Braun, H.-J. Hansen, *Helv. Chim. Acta* **1991**, *74*, 79–90; b) R. Schmidt, C. Tanielan, R. Dunsbach, C. Wolff, *J. Photochem. Photobiol. A* **1994**, *79*, 11–17; c) C. Martí, O. Jürgens, O. Cuenca, M. Casals, S. Nonell, *J. Photochem. Photobiol. A* **1996**, *97*, 11–18; d) E. Oliveros, S. H. Bossmann, G. Heit, G. Troescher, A. Neuner, C. Martínez, A. M. Braun, C. Martí, S. Nonell, *New J. Chem.* **1999**, *23*, 85–93.
- [31] M. Boneva, S. K. Ivanov, E. Oliveros, A. M. Braun, *J. Photochem. Photobiol. A* **1992**, *68*, 343–351, and references cited therein.
- [32] E. Oliveros, P. Murasecco-Suardi, A. M. Braun, H.-J. Hansen, *Methods Enzymol.* **1992**, *213*, 420–429.
- [33] Gas hourly space velocity (GHSV, h^{-1}) is defined as the ratio of the flow rate ($\text{m}^3 \text{h}^{-1}$) on the catalyst volume (m^3). This parameter is more relevant in the case of granular material as suggested in *Manual on Catalyst Characterization*, Vol. 63, No. 9 (Ed.: J. Haber), *Pure Appl. Chem.* **1991**, 1227–1249.
- [34] A. A. Abdel-Shafi, P. D. Beer, R. J. Mortimer, F. Wilkinson, *Helv. Chim. Acta* **2001**, *84*, 2784–2795.
- [35] M. I. Gutierrez, C. G. Martinez, D. García-Fresnadillo, A. M. Castro, G. Orellana, A. M. Braun, E. Oliveros, *J. Phys. Chem. A* **2003**, *107*, 3397–3403.
- [36] D. C. Dobrowolski, P. R. Ogilby, C. S. Foote, *J. Phys. Chem.* **1983**, *87*, 2261–2263.
- [37] E. L. Clennan, D. Wang, H. Zhang, C. H. Clifton, *Tetrahedron Lett.* **1994**, *35*, 4723–4726.
- [38] G. J. Kavarnos, N. J. Turro, *Chem. Rev.* **1986**, *86*, 401–449.
- [39] L. Ma, X. Wang, B. Wang, J. Chen, J. Wang, K. Huang, B. Zhang, Y. Cao, Z. Han, S. Qian, S. Yao, *Chem. Phys.* **2002**, *285*, 85–94.
- [40] F. Cermola, M. DellaGreca, M. R. Ilesca, S. Montella, A. Pollio, F. Temussi, *Chemosphere* **2004**, *55*, 1035–1041.
- [41] H. Goerner, *Photochem. Photobiol. Sci.* **2006**, *5*, 1052–1058.

Received: July 17, 2007

Published online on October 19, 2007